Cell

The Structural Basis for the Large Powerstroke of Myosin VI

Julie Ménétrey,[1,3] Paola Llinas,[1,3] Monalisa Mukherjea,[2] H. Lee Sweeney,[2,*] and Anne Houdusse[1,*]
[1]Structural Motility, Institut Curie CNRS, UMR144, 26 rue d'Ulm, 75248 Paris cedex 05, France
[2]Department of Physiology, University of Pennsylvania School of Medicine, 3700 Hamilton Walk, Philadelphia, PA 19104, USA
[3]These authors contributed equally to this work.
*Correspondence: lsweeney@mail.med.upenn.edu (H.L.S.), anne.houdusse@curie.fr (A.H.)
DOI 10.1016/j.cell.2007.08.027

SUMMARY

Due to a unique addition to the lever arm-positioning region (converter), class VI myosins move in the opposite direction (toward the minus-end of actin filaments) compared to other characterized myosin classes. However, the large size of the myosin VI lever arm swing (powerstroke) cannot be explained by our current view of the structural transitions that occur within the myosin motor. We have solved the crystal structure of a fragment of the myosin VI motor in the structural state that represents the starting point for movement on actin; the pre-powerstroke state. Unexpectedly, the converter itself rearranges to achieve a conformation that has not been seen for other myosins. This results in a much larger powerstroke than is achievable without the converter rearrangement. Moreover, it provides a new mechanism that could be exploited to increase the powerstroke of yet to be characterized plus-end-directed myosin classes.

INTRODUCTION

Within the myosin superfamily there are at least 20 classes of molecular motors that move along actin filaments (Berg et al., 2001). Myosin motor activity is initiated by binding to actin in a state known as the pre-powerstroke state, in which the ATP hydrolysis products are trapped. Actin binding drives conformational changes that allow sequential release of P_i and MgADP, and is coupled to movement of the myosin "lever arm." The lever arm is a variable length, extended alpha-helix containing calmodulin (CaM) and/or CaM-like light chain binding sites (IQ motifs). It is attached to a subdomain of the myosin motor known as the converter. The converter itself is thought to rotate as a rigid body, rectifying and amplifying the structural changes within the motor domain. The final position of the lever arm at the end of the powerstroke is reached in the actin-myosin rigor conformation, which is formed following the release of ADP. Thus the magnitude of the myosin powerstroke, often referred to as the stroke size, is determined by the net displacement at the end of the lever arm from its pre-powerstroke position to its rigor position. This structure-based explanation of myosin motor activity is referred to as the swinging lever arm hypothesis (Holmes and Geeves, 2000; Holmes et al., 2004) and is illustrated in Figure 1A.

Myosin VI is the only class of myosin that has been shown to move toward the minus-end of actin filaments (Wells et al., 1999). The myosin VI dimer is capable of processive movement (i.e., can move as a single molecule) along an actin filament (Park et al., 2006) as well as load dependent anchoring (Altman et al., 2004), and thus can fulfill a number of specialized cell biological functions (Buss et al., 2004; Frank et al., 2004; Sweeney and Houdusse, 2007). Underlying its unusual properties are two unique structural inserts within the myosin VI motor. The first of these, insert 1, is near the nucleotide-binding site and is responsible for gating of the myosin VI heads during processive movement, and likely is necessary for anchoring under high loads (Sweeney et al., 2007). The second insert, insert 2, is a structural extension of the converter subdomain and repositions the myosin VI lever arm (Ménétrey et al., 2005). The first part (proximal helix) of insert 2 interacts with the converter, whereas the second part binds Ca^{2+}-calmodulin. Insert 2 is solely responsible for the reversal of myosin VI directionality, as its removal causes myosin VI to become a plus-end directed motor on actin (Park et al., 2007; Bryant et al., 2007).

The structure of a truncated myosin VI with its CaM-containing lever arm (MD-IQ) in a rigor-like state (a state similar in motor conformation to that believed to exist in the actin-myosin rigor complex) revealed the need for additional adaptations in the myosin VI structure to account for the observed movements of the motor (Ménétrey et al., 2005). The problem is that based on the rigor-like conformation of the myosin VI motor at the end of the powerstroke, and modeling of a pre-powerstroke converter positioning based on myosin I or myosin II structures, the predicted stroke size of the myosin VI MD-IQ would be ~2.5 nm (Figure 1B and Figure S1 in the Supplemental Data available with this article online). However, the stroke size measured in an optical trap is 11–12 nm (Rock et al.,

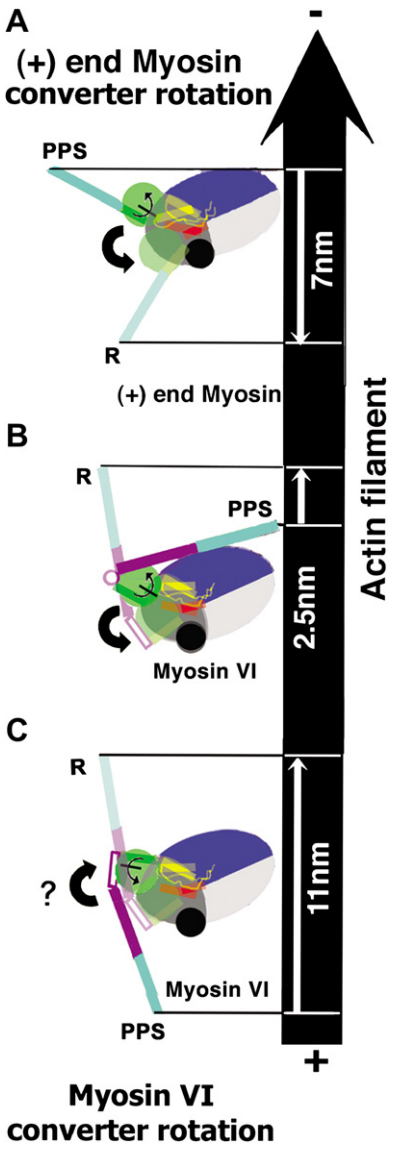

Figure 1. The Swinging Lever Arm Hypothesis and the Problem Posed by Myosin VI

(A) The top panel illustrates the powerstroke of a (+) end-directed myosin, based on structures of scallop myosin II (Houdusse et al., 2000; Yang et al., 2007). From the pre-powerstroke (PPS) and rigor structures, a stroke of 7 nm is predicted for a construct truncated after one light chain/calmodulin-binding site (IQ motif). This corresponds to what has been measured for a truncated myosin V construct with one IQ motif (Purcell et al., 2002). Note that if the lever arm were made longer, as in the case of myosin V, the measured powerstroke (stroke size) would increase (Purcell et al., 2002).

(B) This hypothetical model of the myosin VI powerstroke was generated using the same converter rotation and conformation for myosin VI as that found for plus-end motors, while maintaining the interactions found in rigor between the myosin VI converter and insert 2. Note that the lever arm is predicted to be oriented toward the actin filament, and a stroke of only 2.5 nm is predicted.

(C) To generate the 11–12 nm measured stroke size for myosin VI, the orientation of the converter in the pre-powerstroke state must greatly differ from that of plus-end motors. Note in particular how the orientation of the proximal helix of insert 2 (white cylinder with purple contours) differs from the predicted model (B).

2005), which would necessitate the lever arm movement depicted in Figure 1C. Furthermore, for optimal movement the lever arm swing of myosins should be roughly parallel to the actin filament, which would require a very different position for the lever arm in the pre-powerstroke conformation of myosin VI than would be predicted. In order to account for the observed stroke size of myosin VI, we noted that the lever arm would need to be positioned approximately 180° from its rigor position when in the pre-powerstroke state (Ménétrey et al., 2005 and schematized in Figure 1C), which was also the conclusion based on stroke size measurements involving a series of truncations of the myosin VI lever arm and insert 2 (Bryant et al., 2007). Additionally, earlier studies of full-length monomeric myosin VI led to the conclusion that the rotation of the lever arm would have to be at least 140° to explain the observed stroke size (Lister et al., 2004).

We offered two types of models that could account for this discrepancy (Ménétrey et al., 2005). The first involved an uncoupling of the lever arm in the pre-powerstroke state, and the second called for a unique pre-powerstroke structure. Later experiments ruled out the former and suggested that myosin VI must indeed adopt a different conformation at the beginning of its powerstroke on actin (Park et al., 2007; Bryant et al., 2007). Using a truncation of the myosin VI motor in which the CaM-binding region of insert 2 was removed, we have now solved the pre-powerstroke structure of the myosin VI motor (Figure 2). This structure reveals a number of previously unseen structural adaptations that create a unique pre-powerstroke state and explain the large stroke size observed for myosin VI. Furthermore it demonstrates that one assumption of the swinging lever arm hypothesis, that the converter subdomain of the motor always rotates as a rigid structure, is not correct for all classes of myosin.

RESULTS

Design of the Construct

The pre-powerstroke structures of myosin II and myosin I isoforms have been solved with MgADP and phosphate analogs (either AlF_4 or vanadate) trapped at the nucleotide-binding site of the protein (Fisher et al., 1995; Smith and Rayment, 1996; Dominguez et al., 1998; Houdusse et al., 2000; Kollmar et al., 2002). We were unsuccessful in attempts to crystallize these trapped forms of our previously published truncations (MD-IQ and $MD^{Insert\ 2}$) of myosin VI (Ménétrey et al., 2005), so we further truncated the motor (after isoleucine 789), removing the calmodulin-binding site of insert 2, creating a motor domain (MD) construct.

The function of this myosin VI MD construct was assessed by actin-activated ATPase activity at 25°C. The maximal steady state activity was slightly reduced as

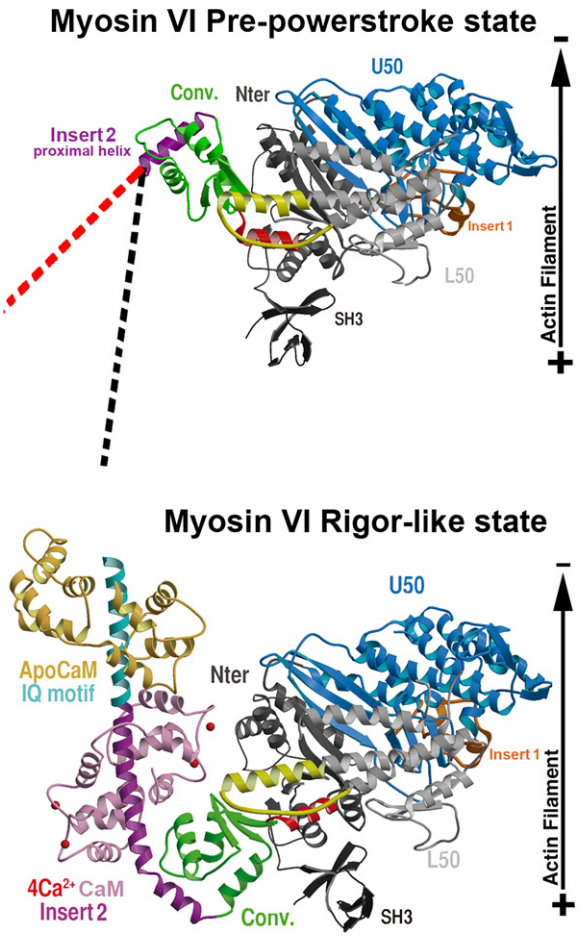

Figure 2. The Myosin VI Pre-Powerstroke Structure Reveals that a Converter Rearrangement Increases the Size of the Powerstroke

The structure of the myosin VI motor domain prior to force generation (pre-powerstroke [PPS]) is compared to that at the end of the powerstroke (rigor-like state). Note the drastic change in the converter (green) position and in the insert 2 proximal helix (purple) orientation. Possible positions of the full lever arm in the pre-powerstroke state are indicated by the red and black dotted lines. The black dotted line indicates that the kink observed in the insert 2 helix in the rigor-like state (below) is maintained in the pre-powerstroke state. The red dotted line indicates the lever arm position if there is no kink in the insert 2 helix in the pre-powerstroke state. This introduces approximately a 40° uncertainty in the lever arm position in the pre-powerstroke state.

compared to MD-IQ (4.6 ± 0.3 s^{-1} and 5.7 ± 0.4 s^{-1}, respectively), with no change in the apparent actin affinity (K_{ATPase}). This was due to a 20% slowing of ADP release in the truncated construct (4 s^{-1} versus 5 s^{-1}). However, truncation clearly did not interfere with the ability of the motor to go through its ATPase cycle on actin. Furthermore, a similarly truncated construct (after serine 791) has previously been shown to have motor activity using a gliding actin filament assay, and also was shown to have decreased ADP release kinetics (Bryant et al., 2007).

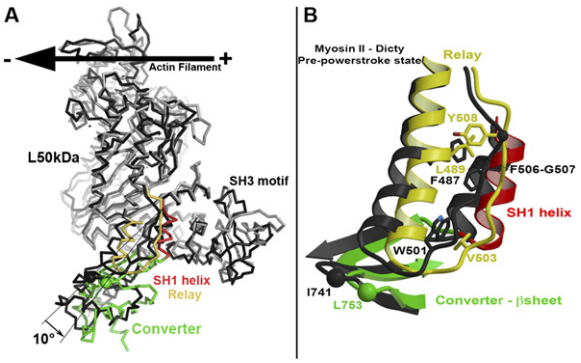

Figure 3. The Myosin VI Converter Is Less "Primed" in the Pre-Powerstroke State

(A) The pre-powerstroke state of myosin VI (color) is compared to that of *Dictyostelium* myosin II (black), with the Lower 50 kDa subdomains superimposed. The structures are oriented relative to a horizontal actin filament (black arrow). Note the difference in the relay (yellow) conformation, which is less bent in myosin VI. This results in a 10° difference in the orientation of the converter (green for myosin VI with L753 indicated as a green ball, the equivalent residue I741 in *Dictyostelium* is indicated as a black ball). Thus, the converter of myosin VI is less "primed" than that of plus-end motors.

(B) Sequence differences at three critical locations in the relay result in the reduction in the myosin converter rotation. Less bulky side chains are found at the beginning of the relay near the helix bend (L489 in myosin VI, F484 in myosin II) and at the relay tip (V503 in myosin VI, W501 in myosin II). Also a one-residue deletion is found at the end of the relay (Y508 in myosin VI, F506-G507 in myosin II). All of these sequence differences contribute to diminishing the steric clash between the relay and the SH1 helix in myosin VI. Thus the relay is not forced to bend as much in myosin VI and the relay main chain is found closer to the SH1 helix than in myosin II.

A Unique Pre-Powerstroke State Increases the Myosin VI Stroke Size

The myosin VI MD construct crystallized in a state with MgADP.vanadate trapped in the nucleotide-binding pocket. The crystals diffracted up to 1.75Å, allowing determination of the myosin VI pre-powerstroke structure at high resolution. As shown in Figure 2, this myosin VI pre-powerstroke structure would position the lever arm greater than 140° from the previously seen rigor-like position, as compared to the 70° rotation seen for myosin II (Houdusse et al., 2000). While the exact lever arm position cannot be determined from this truncated structure, the dotted lines in Figure 2 delineate a range of possible positions. Even with the smallest rotation (red dotted line), the stroke size is clearly much larger than that predicted by previously seen rearrangements in myosin pre-powerstroke structures (see Figure 1B). This is despite the fact that, as shown in Figure S2, the majority of the motor is positioned as in the myosin II pre-powerstroke structures. The exceptions involve the elements that position the converter (known as the relay and SH1 helix) and the converter itself, which is in a previously unseen conformation (Figures 3 and 4).

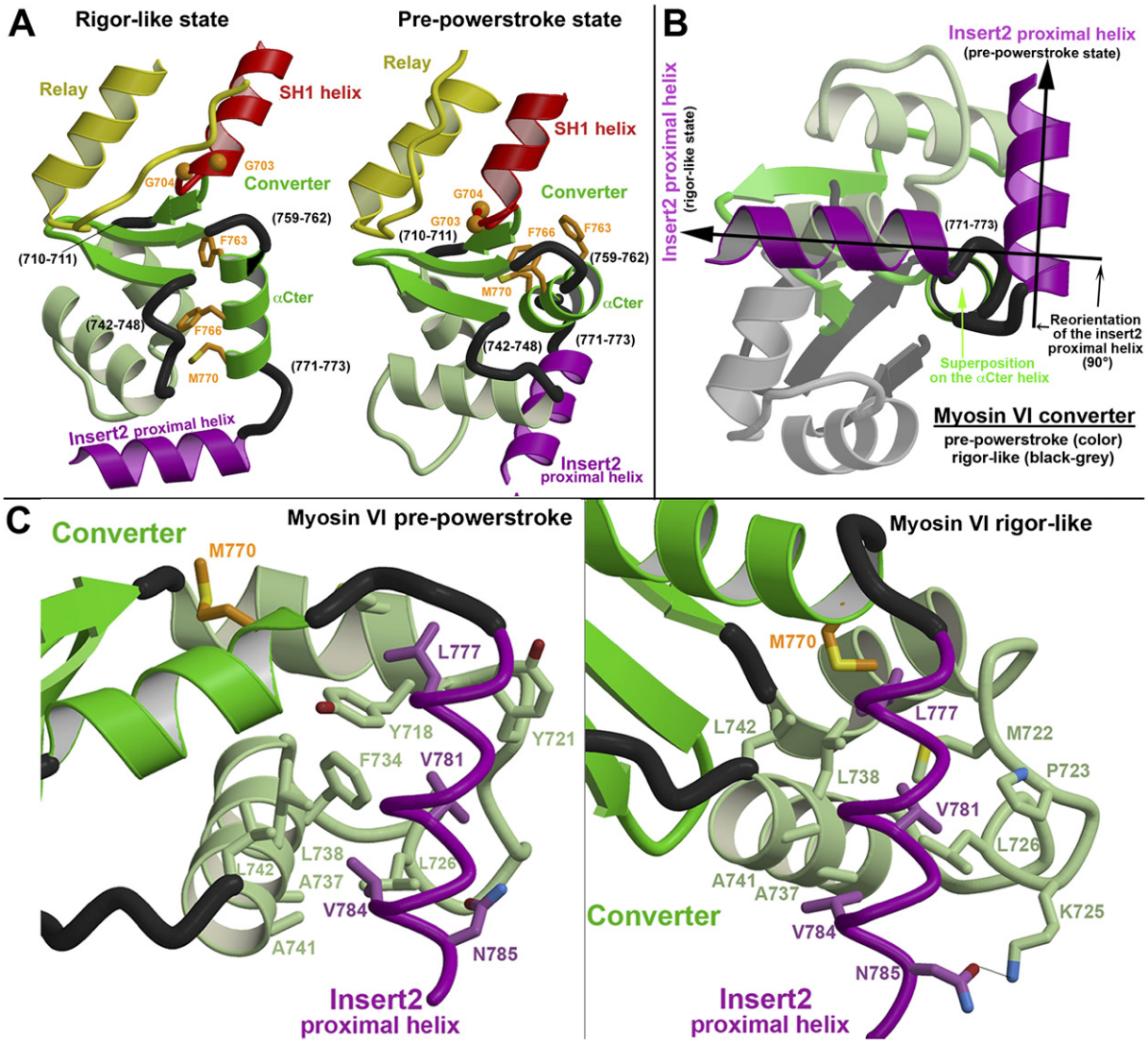

Figure 4. A New Conformation of the Converter Reorients Insert 2 in the Pre-Powerstroke State

(A) The rigor conformation of the converter (left) is compared to that of the pre-powerstroke state (right). In the two structures, the beta sheet is found in a similar orientation and the interactions with the relay and the SH1 helix are mostly conserved. In contrast, four hinges (black) drastically change conformation and reorient the helices of the converter as well as the insert 2 proximal helix (purple). The helix-loop-helix motif (light green) found between the first and the second hinges moves as a rigid body. Note in particular how a drastic conformational change in the third hinge reorients the last helix of the converter (αCter). Three hydrophobic side chains (orange) buried within the converter in the rigor conformation are repositioned toward the surface of the molecule in the pre-powerstroke state. Note also that the SH1 helix unwinds at its C terminus (Gly703-Gly704) in the pre-powerstroke state (shown as orange balls).

(B) An important change in the conformation of the last hinge (residues 771–773) allow the orientation of the proximal helix of insert 2 to differ by ~90° (relative to the αCter helix) between the pre-powerstroke state (color) and the rigor state (gray).

(C) Comparison of the docking site of the insert 2 proximal helix (purple) in the two converter conformations. The same surface of this helix (L777-V780-V784-N785) interacts very differently in the two structures, mainly with the helix-loop-helix motif (light green) of the converter.

An Altered Conformation of the Relay Repositions the Converter

It is clear that "priming" of the lever arm at the beginning of the power stroke is accomplished in part by a bending of a helix contained within a region known as the relay, which in turn interfaces with the converter. As recently modeled (Koppole et al., 2006), a steric clash between another structural element that connects to the converter, the SH1 helix, causes the bending of the relay helix and thus priming of the lever arm. As shown in Figure 3, substitution of bulky side chains in the relay of myosin VI lessens this steric clash, allowing its relay to be closer to the SH1 helix. This decreases the bending of the relay helix as compared with the relay of myosin II, resulting in a 10° difference in

the amount of converter rotation, such that the myosin VI converter is less "primed" toward the minus-end of an actin filament in the pre-powerstroke state than is a plus-end directed motor. This helps increase the stroke size, since in its pre-powerstroke state, the myosin VI lever arm needs to be positioned toward the plus-end of the actin filament.

A New Conformation of the Converter Repositions the Lever Arm in the Pre-Powerstroke State

While the 10° repositioning of the converter due to the altered relay conformation contributes to the repositioning of the lever arm, the main structural adaptation underlying the large myosin VI stroke size is a rearrangement of the converter itself. Such a rearrangement has not been seen for any other myosin converter, and is possible due to myosin VI-specific structural adaptations illustrated in Figure 4. Note that the interfaces between the converter and the relay and SH1 helices are conserved, demonstrating that the converter remains tightly coupled to the motor during its rearrangements. However all of the helices of the converter reorient in the pre-powerstroke conformation, including the first (proximal) helix of insert 2, which rotates by ~90° relative to the last helix of the converter. While we have previously suggested that insert 2 might uncouple from the converter in the pre-powerstroke state, this structure suggests that instead it remains tightly coupled, but is reoriented by the overall converter conformational change. As highlighted in Figure 4, the relative movements of the converter helices are made possible by four flexible linkers or hinges (shown in black) and by hydrophobic surfaces on which rotation of the helices can occur. The combination of the 90° rotation of the insert 2 proximal helix within the converter, the 25° rotation of the last helix of the converter, and the overall converter rotation of about 60° between pre-powerstroke state and rigor, accounts for a minimal lever arm rotation of ~140°, as indicated in Figure 2. Based on modeling presented below, interactions between the lever arm and the converter may contribute to the exact position adopted by the lever arm (Figure 5A).

Modeling the Complete Myosin VI Lever Arm onto the Pre-Powerstroke Structure

In order to provide a better estimate of the stroke size predicted by the pre-powerstroke structure, we modeled the full myosin VI lever arm onto the structure. The model of the lever arm of the myosin VI pre-powerstroke structure was obtained by superimposing the final residues of the insert 2 proximal helix present in the MD structure (residues 785–788) with those of the myosin VI MD-IQ rigor-like state structure (2BKI; Ménétrey et al., 2005). A small adjustment of the lever arm orientation allowed positioning of the lever arm so that contacts could be formed between the converter and the N-terminal lobe of the calmodulin as exist in the rigor-like structure (Figure 5A). Note that in this model, the myosin VI lever arm is oriented roughly parallel to the actin filament, pointing toward the plus-end. The model results in a lever-arm rotation of ~180° from pre-powerstroke to rigor, accounting for a movement of 11–12 nm at the end of the lever arm (Figure 5B). If contacts between the converter and CaM are not formed, then the rotation would be somewhat less (>140°), and the lever arm would likely be highly mobile in the pre-powerstroke state. Only the full 180° rotation correctly predicts the measured stroke size for the construct with the full myosin VI lever arm (Rock et al., 2005). Furthermore, as noted in Figure 5B, the modeled position of the pre-powerstroke lever arm provides correct predictions for the directionality and reasonable predictions for the stroke sizes of the series of truncated myosin VI constructs characterized by Bryant et al. (2007). Any model that decreases the rotation of the lever arm will lead to increasing discrepancies between measured and predicted stroke sizes. Note that in any event, as illustrated in Figure 5C, this large stroke size cannot entirely account for the observed myosin VI step size of 30–36 nm (Park et al., 2006; Rock et al., 2001; Nishikawa et al., 2002) without some extension of the lever arm, as previously proposed (Rock et al., 2005).

DISCUSSION

An important question is what drives the converter to alter its conformation from the new form seen in the pre-powerstroke, to the more conventional folding seen in the rigor conformation of myosin VI and in all other myosins. Illustrated in Figure 6 is a model demonstrating that the conventional (rigor) conformation of the myosin VI converter can be accommodated in the pre-powerstroke structure (but as previously noted, would reduce the stroke size). However, as also illustrated in Figure 6, the unusual (pre-powerstroke) converter conformation cannot be accommodated in the myosin VI rigor-like structure due to a steric clash with the N-terminal subdomain of the motor. Furthermore, the rigor converter conformation is stabilized by specific interactions with the N-terminal subdomain of myosin VI (Figure 6B). These observations suggest that the pre-powerstroke converter conformation is favored in the absence of constraints, and likely exists in the initial states of the powerstroke. It must be forced out of this conformation and into the conventional conformation later in the cycle, prior to formation of the rigor complex on actin. Indeed, the relatively large heat capacity and enthalpy changes seen with ADP binding to actomyosin VI (Robblee et al., 2005) could be indicative of converter rearrangements.

In addition to creating a larger stroke size, the converter rearrangements of myosin VI could be influenced by strain, and therefore be exploited for fine-tuning of cellular functions. A recent study demonstrated that during processive movement gating of the lead head of a myosin VI dimer is accomplished by preventing ATP binding (Sweeney et al., 2007). At the same time, and unlike the gating for myosin V, ADP release is unaffected (Sweeney et al., 2007). This appears to be accomplished by rearward

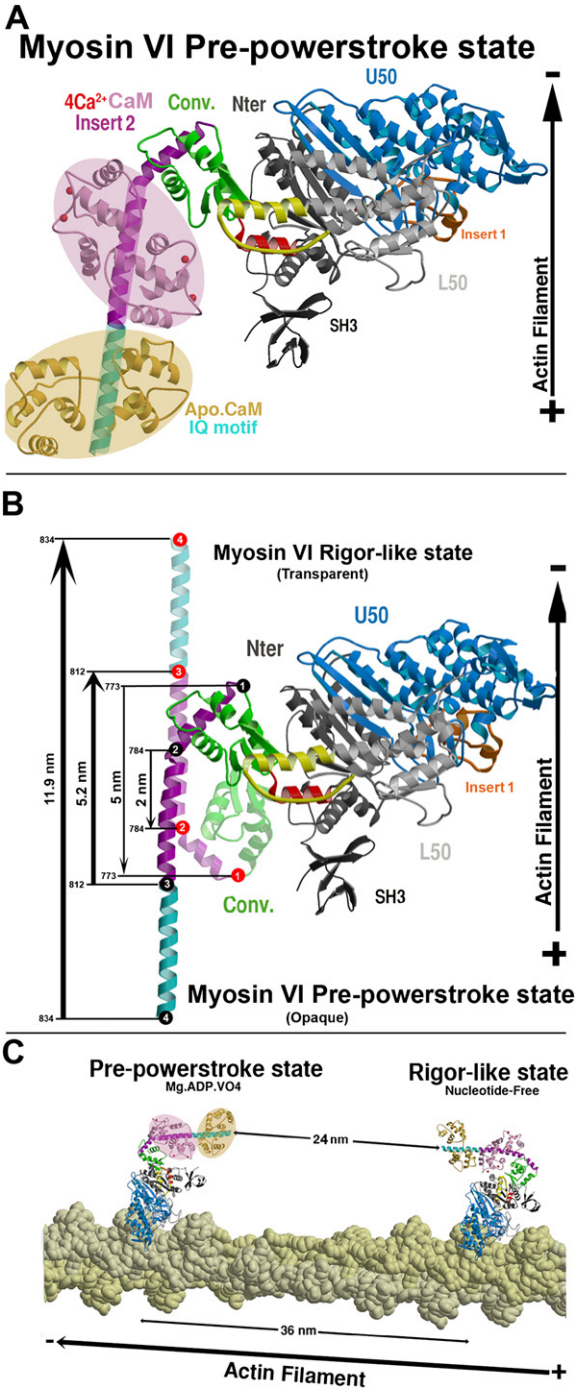

Figure 5. Modeling the Lever Arm onto the Myosin VI Pre-Powerstroke (PPS) Structure Explains the Large Stroke Size of Myosin VI

(A) The structure of myosin VI prior to force generation (pre-powerstroke [PPS]) is shown with a model for the position of the myosin VI lever arm. The lever arm, consisting of the Ca^{2+}-CaM-binding region of insert 2 (purple), and the IQ motif with its associated CaM, were not present in the truncated protein and thus were modeled in the PPS structure (based on the rigor-like structure shown in Figure 2). As in the rigor-like structure, the lever arm was positioned to allow strain positioning insert 1 in the lead head of the myosin VI dimer so that it restricts the entry of the gamma phosphate of ATP, but does not restrict ADP entry or release. One observation of the study that was difficult to understand was that once the rear head detaches, relieving the intramolecular strain, there was a significant delay before ATP could bind to the lead head. Based on the converter structure described in this study, one possible explanation is that rearward strain maintains the pre-powerstroke conformation of the converter. Once the strain is relieved, the rate-limiting step for ATP binding to the lead head could be a combination of converter rearrangements that allow the rigor state to form, coupled to insert 1 repositioning.

Another unexplained property of the processive movement of a single dimeric myosin VI molecule along an actin filament is its highly variable step size (Park et al., 2006; Rock et al., 2001; Nishikawa et al., 2002). While it has been proposed that this variability might be due to a flexible lever arm extension (Rock et al., 2005), much of the source of the variability recently was shown to reside within the myosin VI motor domain (Park et al., 2007). This is based on the observation that when the lever arm and coiled coil of myosin V were appended to the last helix of the myosin VI converter, the step size of the plus-end directed chimeric dimer displayed as much variability as for wild-type myosin VI (Park et al., 2007). Thus the possibility that the converter of the rear head of a processive myosin VI dimer might be undergoing a transition from its pre-powerstroke to rigor conformation, and thus be in either of its two conformations while the unattached lead head is searching for an actin binding site, could contribute to the highly variable step size.

The pre-powerstroke structure presented herein correctly predicts the measured myosin VI stroke size and obviates the need to postulate any type of uncoupling

interactions between the N-terminal lobe of the insert 2 Ca^{2+}-CaM and the converter. However, the exact interactions found in the rigor-like state between Ca^{2+}-CaM and the converter cannot be conserved in the PPS since the converter folding is different.

(B) To visualize the stroke of myosin VI, the myosin VI pre-powerstroke structure with modeled lever arm is overlaid on the rigor-like structure after superimposing the lower 50 kDa domains of the two structures. The calmodulins are omitted for clarity. The new myosin VI pre-powerstroke structure with the modeled lever arm, together with the rigor-like structure, predict an ~12 nm powerstroke toward the minus end of the filament for myosin VI with its two calmodulin-containing lever arm, in agreement with what has been measured (Rock et al., 2005). (This is labeled as position 4 on the lever arm.) The stroke sizes of truncated constructs characterized by Bryant et al. (2007) are indicated at lever arm lengths labeled 1–3. The measured directionality and stroke sizes for these constructs were: (1) +2 nm, (2) +2 nm, and (3) −7nm to −9 nm. As indicated in the figure, the structure-based predictions of directionality and stroke sizes are: (1) +5 nm, (2) +2 nm, and (3) −5.2 nm.

(C) The myosin VI pre-powerstroke and rigor-like structures are docked on an actin filament with a 36 nm step separation between them, consistent with the measured step size of a full-length myosin VI dimer (Park et al., 2007). The distance between the ends of the two lever arms is large (24 nm), indicating that an extension of the lever arm must exist to connect them, as has been shown experimentally (Rock et al., 2005).

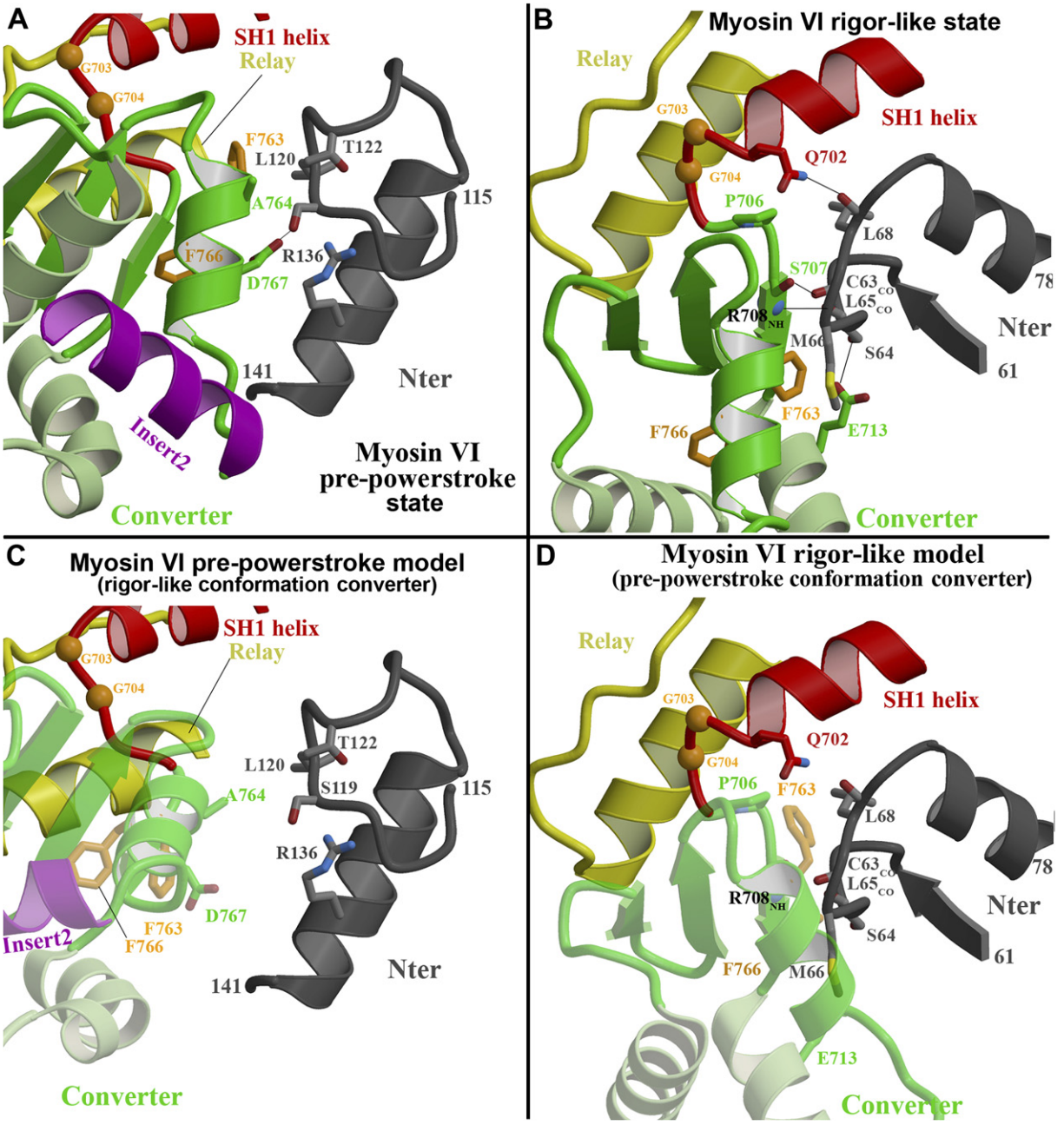

Figure 6. Converter/N-terminal Subdomain Interactions

The position of the converter may also be influenced by the interactions it makes with the N-terminal subdomain. These interactions are weak in the case of the pre-powerstroke structure (A) but they are quite important in the rigor state (B). Note that the surface of the N-terminal subdomain involved in each case is different. Since the converter/relay interface is similar in both structures, it is possible to model the rigor converter conformation in the pre-powerstroke state (C) and the pre-powerstroke converter conformation in the rigor structure (D). It is clear that the rigor converter conformation is compatible with the pre-powerstroke structure but would not allow any interactions to be made with the N-terminal subdomain (C). In contrast, the pre-powerstroke conformation is incompatible with the rigor structure since a large steric clash would occur between the converter and the N-terminal subdomain (D). Thus, it seems that the unusual pre-powerstroke folding of the converter would be favored by myosin VI in the absence of constraints. Rearrangement to create the rigor folding, which is the one most similar to that of plus-end motors, may be triggered near the end of the working stroke by converter/N-terminal subdomain interactions.

involving either the converter or insert 2. Rather, the converter and insert 2 can maintain connectivity while reorienting their helices. Although converter rearrangements of this sort have not been observed for myosin II or myosin I and have not previously been considered in the swinging lever arm hypothesis, such rearrangements

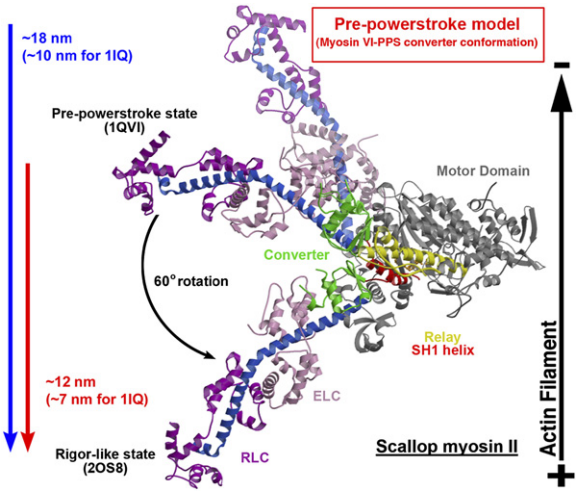

Figure 7. The Myosin VI Pre-Powerstroke Converter Conformation Would Increase the Stroke Size of a Plus-End-Directed Myosin

Using a pre-powerstroke (1QVI; Gourinath et al., 2003) and a rigor-like structure (2OS8; Yang et al., 2007) for scallop myosin II, the predicted stroke size with the full myosin II lever arm (containing two calmodulin-like myosin light chains) is 12 nm. (This is reduced to 7 nm for a single IQ-containing lever arm, as in Figure 1A.) This is compared to the predicted stroke size based on modeling the myosin VI pre-powerstroke converter into the scallop pre-powerstroke structure. In this model, the pre-powerstroke lever arm position would be moved further toward the (–) end of the actin filament, and more parallel with the actin filament, increasing the predicted stroke size to 18 nm (10 nm for a single IQ-containing lever arm). While it is clear that this converter rearrangement mechanism is not used by myosin II, we propose that in addition to myosin VI, it may be used by classes of unconventional myosins that have yet to be characterized in order to create larger powerstrokes.

could give rise to larger stroke sizes in the case of plus-end directed myosins. This is illustrated in the model shown in Figure 7, in which the stroke size of scallop myosin II with its complete lever arm would be increased by 50% (from 12 nm to 18 nm) using the pre-powerstroke converter rearrangement found in myosin VI. (This also can be visualized in Figure S1 by noting that the position of the last helix of the converter of myosin VI moves in a plus-end directed manner, consistent with recent studies [Park et al., 2007; Bryant et al., 2007]. However, the magnitude of this plus-end directed movement is larger than if the converter rearrangement did not occur.) While the unitary displacement (stroke size) increases with lever arm length, the unitary force decreases. Since the converter rearrangement mechanism of myosin VI generates larger movements without the need to increase the length of the lever arm, it may offer a better compromise between maximizing force production and stroke size. Thus it is possible that some classes of plus-end directed myosins that have yet to be examined in detail might use a similar scheme of converter rearrangements to amplify the size of their movements.

EXPERIMENTAL PROCEDURES

Protein Constructs, Expression, and Functional Assays

To create the myosin VI MD construct used to obtain crystals, the porcine myosin VI cDNA was truncated after isoleucine 789. This truncation is at the end of the first (proximal) helix of insert 2, and precedes the CaM-binding site of insert 2. A Flag tag (encoding GDYKDDDDK) was appended to the N-terminus to allow for purification. The construct was used to create a recombinant baculovirus and express protein in SF9 cells, as previously described (Sweeney et al., 1998). ATPase assays and ADP release from actomyosin VI measurements were performed as previously described (De La Cruz et al., 2001).

Crystallization and Data Collection

Crystals of myosin VI MD were obtained by vapor diffusion method with spontaneous nucleation occurring at 18°C in hanging drops using equal amounts of reservoir solution (containing 3%–4% PEG 8000, 50 mM MES [pH 6.75], 100 mM SAM, 1 mM TCEP) and stock solution of the protein at 6–8 mg/ml. Prior to freezing and data collection, the crystals were transferred into a final cryoprotectant solution containing 8% PEG 8000 with 20% Ethylene glycol. X-ray data sets were collected at 100 K on the ID23-1 beamline of the European Synchrotron Radiation Facility. Data sets were integrated with MOSFLM (Collaborative Computational Project, Number 4, 1994) and scaled with SCALA (Collaborative Computational Project, Number 4, 1994). See Table S1 for statistics on the data collection.

Structural Determination and Refinement

The myosin VI structure was solved by molecular replacement with the program AmoRe (Navaza, 1994) at 3.0 Å resolution using a myosin VI pre-powerstroke state polyalanine model (superposition of the N-terminal, the upper and lower 50kda subdomains of myosin VI rigor-like structure (Ménétrey et al., 2005:PDB code 2BKH) on those of the myosin II *Dictyostelium discoideum* pre-powerstroke structure (Smith and Rayment, 1996: PDB code 1VOM). The SH3 subdomain and the side chains were manually built and refined with Refmac5 (Collaborative Computational Project, Number 4, 1994). Overall refinement and water/heterogen molecule attribution were then carried out at 1.75 Å resolution with Refmac5 (Collaborative Computational Project, Number 4, 1994) and Coot (Emsley and Cowtan, 2004). See Table S1 for statistics on the structural refinement. Note that all figures were computed using MOLSCRIPT (Kraulis, 1991) with Raster3D rendering (Merritt and Bacon, 1997).

Supplemental Data

Supplemental Data include two figures, one table, and a movie and can be found with this article online at http://www.cell.com/cgi/content/full/131/2/300/DC1/.

ACKNOWLEDGMENTS

We are grateful to Anna Li and Xiaoyan Liu for protein purification and to Alan B. Zong for performing ATPase assays. We also thank Jerome Cicolari for assistance with crystallization and X-ray data collection. This work was supported by grants from NIAMS (National Institute of Arthritis and Musculoskeletal and Skin Diseases) and NIDCD (National Institute of Deafness and other Communication Disorders) (H.L.S.), the CNRS (Centre Nationale de la Recherche Scientifique) (A.H.), the ANR (Agence Nationale de la Recherche) (A.H.), and the ACI BCMS (Action Concertée Incitative Biologie Cellulaire, Moléculaire et Structurale) (A.H.).

Received: June 10, 2007
Revised: August 7, 2007
Accepted: August 15, 2007
Published: October 18, 2007

REFERENCES

Altman, D., Sweeney, H.L., and Spudich, J.A. (2004). The mechanism of myosin VI translocation and its load-induced anchoring. Cell *116*, 737–749.

Berg, J.S., Powell, B.C., and Cheney, R.E. (2001). A millennial myosin census. Mol. Biol. Cell *12*, 780–794.

Buss, F., Spudich, G., and Kendrick-Jones, J. (2004). Myosin VI: Cellular Functions and motor properties. Annu. Rev. Cell Dev. Biol. *20*, 649–676.

Bryant, Z., Altman, D., and Spudich, J.A. (2007). The power stroke of myosin VI and the basis of reverse directionality. Proc. Natl. Acad. Sci. USA *104*, 772–777.

Collaborative Computational Project, Number 4 (1994). The CCP4 suite: program for protein crystallography. Acta Crystallogr. *D50*, 760–763.

De La Cruz, E.M., Ostap, E.M., and Sweeney, H.L. (2001). Kinetic mechanism and regulation of myosin VI. J. Biol. Chem. *276*, 32373–32381.

Dominguez, R., Freyzon, Y., Trybus, K.M., and Cohen, C. (1998). Crystal structure of a vertebrate smooth muscle myosin motor domain and its complex with the essential light chain: visualization of the pre-power stroke state. Cell *94*, 559–571.

Emsley, P., and Cowtan, K. (2004). Coot: model-building tools for molecular graphics. Acta Crystallogr. D Biol. Crystallogr. *60*, 2126–2132.

Fisher, A.J., Smith, C.A., Thoden, J.B., Smith, R., Sutoh, K., Holden, H.M., and Rayment, I. (1995). X-ray structures of the myosin motor domain of *Dictyostelium discoideum* complexed with MgADP.BeFx and MgADP.AlF4-. Biochemistry *34*, 8960–8972.

Frank, D.J., Noguchi, T., and Miller, K.G. (2004). Myosin VI: Cellular functions and motor properties. Curr. Opin. Cell Biol. *16*, 189–194.

Gourinath, S., Himmel, D.M., Brown, J.H., Reshetnikova, L., Szent-Gyorgyi, A.G., and Cohen, C. (2003). Crystal structure of scallop Myosin S1 in the pre-power stroke state to 2.6 Å resolution: flexibility and function in the head. Structure *11*, 1621–1627.

Holmes, K.C., and Geeves, M.A. (2000). The structural basis of muscle contraction. Philos. Trans. R. Soc. Lond. B Biol. Sci. *355*, 419–431.

Holmes, K.C., Schroder, R.R., Sweeney, H.L., and Houdusse, A. (2004). The structure of the rigor complex and its implications for the power stroke. Philos. Trans. R. Soc. Lond. B Biol. Sci. *359*, 1819–1828.

Houdusse, A., Szent-Györgyi, A., and Cohen, C. (2000). Three conformational states of scallop myosin subfragment S1. Proc. Natl. Acad. Sci. USA *97*, 11238–11243.

Kollmar, M., Durrwang, U., Kliche, W., Manstein, D.J., and Kull, F.J. (2002). Crystal structure of the motor domain of a class-I myosin. EMBO J. *21*, 2517–2525.

Koppole, S., Smith, J.C., and Fischer, S. (2006). Simulations of the myosin II motor reveal a nucleotide-state sensing element that controls the recovery stroke. J. Mol. Biol. *361*, 604–616.

Kraulis, P.J. (1991). MOLSCRIPT: a program to produce both detailed and schematic plots of protein structures. J. Appl. Cryst. *24*, 946–950.

Lister, I., Schmitz, S., Walker, M., Trinick, J., Buss, F., Veigel, C., and Kendrick-Jones, J. (2004). A monomeric myosin VI with a large working stroke. EMBO J. *23*, 1729–1738.

Ménétrey, J., Bahloul, A., Wells, A.L., Yengo, C.M., Morris, C.A., Sweeney, H.L., and Houdusse, A. (2005). The structure of the myosin VI motor reveals the mechanism of directionality reversal. Nature *435*, 779–785.

Merritt, E.A., and Bacon, D.J. (1997). Raster3D: Photorealistic Molecular Graphics. Methods Enzymol. *277*, 505–524.

Navaza, J. (1994). AMoRe: an automated package for molecular replacement. Acta Crystallogr. A *50*, 157–163.

Nishikawa, S., Homma, K., Komori, Y., Iwaki, M., Wazawa, T., Hikikoshi Iwane, A., Saito, J., Ikebe, R., Katayama, E., Yanagida, T., and Ikebe, M. (2002). Class VI myosin moves processively along actin filaments backward with large steps. Biochem. Biophys. Res. Commun. *290*, 311–317.

Park, H., Li, A., Chen, L.-Q., Houdusse, A., Selvin, P.R., and Sweeney, H.L. (2007). The unique insert at the end of the myosin VI motor is the sole determinant of directionality. Proc. Natl. Acad. Sci. USA *104*, 778–783.

Park, H., Ramamurthy, B., Travaglia, M., Safer, D., Chen, L.-Q., Franzini-Armstrong, C., Selvin, P.R., and Sweeney, H.L. (2006). Full-length myosin VI dimerizes and moves processively along actin filaments upon monomer clustering. Mol. Cell *21*, 331–336.

Purcell, T.J., Morris, C., Spudich, J.A., and Sweeney, H.L. (2002). Role of the lever arm in the processive stepping of myosin V. Proc. Natl. Acad. Sci. USA *99*, 14159–14164.

Robblee, J.P., Cao, W., Henn, A., Hannemann, D.E., and De La Cruz, E.M. (2005). Thermodynamics of nucleotide binding to actomyosin V and VI: a positive heat capacity change accompanies strong ADP binding. Biochemistry *44*, 10238–10249.

Rock, R.S., Ramamurthy, B., Dunn, A.R., Beccafico, S., Morris, C.A., Spink, B., Rami, B., Franzini-Armstrong, C., Spudich, J.A., and Sweeney, H.L. (2005). A flexible domain is essential for the large step size and processivity of myosin VI. Mol. Cell *17*, 603–609.

Rock, R.S., Rice, S.E., Wells, A.L., Purcell, T.J., Spudich, J.A., and Sweeney, H.L. (2001). Myosin VI is a processive motor with a large step size. Proc. Natl. Acad. Sci. USA *98*, 13655–13659.

Smith, C.A., and Rayment, I. (1996). X-ray structure of the magnesium(II).ADP.vanadate complex of the Dictyostelium discoideum myosin motor domain to 1.9 A resolution. Biochemistry *35*, 5404–5417.

Sweeney, H.L., and Houdusse, A. (2007). What can myosin VI do in cells? Curr. Opin. Cell Biol. *19*, 57–66.

Sweeney, H.L., Park, H., Zong, A.B., Yang, Z., Selvin, P.R., and Rosenfeld, S.S. (2007). How myosin VI coordinates its heads during processive movement. EMBO J. *26*, 2682–2692.

Sweeney, H.L., Rosenfeld, S.S., Brown, F., Faust, L., Smith, J., Stein, L., and Sellers, J. (1998). Kinetic tuning of myosin via a flexible loop adjacent to the nucleotide-binding pocket. J. Biol. Chem. *273*, 6262–6270.

Wells, A.L., Lin, A.W., Chen, L.-Q., Safer, D., Cain, S.M., Hasson, T., Carragher, B.O., Milligan, R.A., and Sweeney, H.L. (1999). Myosin VI is an actin-based motor that moves backwards. Nature *401*, 505–508.

Yang, Y., Gourinath, S., Kovacs, M., Nyitray, L., Reutzel, R., Himmel, D.M., O'Neall-Hennessey, E., Reshetnikova, L., Szent-Gyorgyi, A.G., Brown, J.H., and Cohen, C. (2007). Rigor-like structures from muscle myosins reveal key mechanical elements in the transduction pathways of this allosteric motor. Structure *15*, 553–564.

Accession Numbers

Atomic coordinates and structure factors have been deposited in the Protein Data Bank under the accession numbers 2V26 and r2v26sf, respectively, for the pre-powerstroke structure of the myosin VI motor domain.